# 2
Simulation Methodology

Device simulation is vital in the advancement of any technology, which permits the designers to enhance the design and process flows of the device before sending it to fabrication. While considering the material cost of III-Ns, this phenomenon is also true for AlGaN/GaN HEMTs. This chapter illustrates the simulation methodology, which will be employed to elaborate on the physical properties and electrical behavior of the device. The primary aim of this device simulations is to observe the behavior of AlGaN/GaN HEMT under different operating conditions, which is validated by experimental results. Further, the analysis of AlGaN/GaN HEMT provided in the chapter will illustrate the impact of self-heating on its electrical characteristics. Herein, the *Sentaurus Technology Computer-Aided Design* (TCAD) *simulator tool*, provided by Synopsys Inc., was utilized to perform the analysis. The relevant mathematical and physical models of AlGaN, GaN, and AlN and corresponding parameters provided by Sentaurus TCAD were utilized and modified to observe these characteristics of AlGaN/GaN HEMT. These models and parameters not only time-saving but also confirms precise material characteristics such as piezoelectric polarization. The information related to Sentaurus TCAD will be described at the beginning of this chapter. Later on, the different device physical and mathematical models and charge transport equations will be explained, which provide the framework of the device physics utilized in the simulation. The last part of the chapter will illustrate the device design and the impact of the self-heating effect on the electrical behavior of the device.

2.1 THE SENTAURUS TCAD SIMULATOR

The *Sentaurus TCAD* utilizes the simulations on high-performance computing systems to expresses the development and optimization of the semiconductor devices and processing technologies. The software performs numerical simulation to solve basic physical partial differential equations, like charge transport and diffusion equations, to demonstrate the structural and electrical behavior of the designed device of different semiconductors, including Si, Ge, InN, InAs, GaN, GaAs, and many more. The software package of the *Sentaurus TCAD* offers a wide range of tools that have individual editable input files that allow the user to make full control over the simulation parameters and models to implement these calculations along with visualization supports to perceive the physical properties and behavior in the device. Figure 2.1 shows the process flow employed in this thesis for the *Sentaurus TCAD* device simulation. The tools which were utilized in this work include the *Sentaurus Workbench (SWB)*, *Sentaurus Device Editor (SDE)*, *Sentaurus Device (SDevice)*, *Inspect*, and *Tecplot*. A brief explanation of each tool is explained below.

2.1.1 Sentaurus Workbench (SWB)

The Sentaurus Workbench (SWB) is a primary graphical front-end simulation platform provided by Synopsys, where other tools were integrated. As the name suggests, it offers a user-friendly environment where one can perform the simulation consecutively from the beginning of the design of the device structure to the device operation and analysis. It also offers flexibility to execute simultaneous simulations on the device by utilizing the variation in the physical and structural properties' parameters to visually analyze device characteristics and behavior.
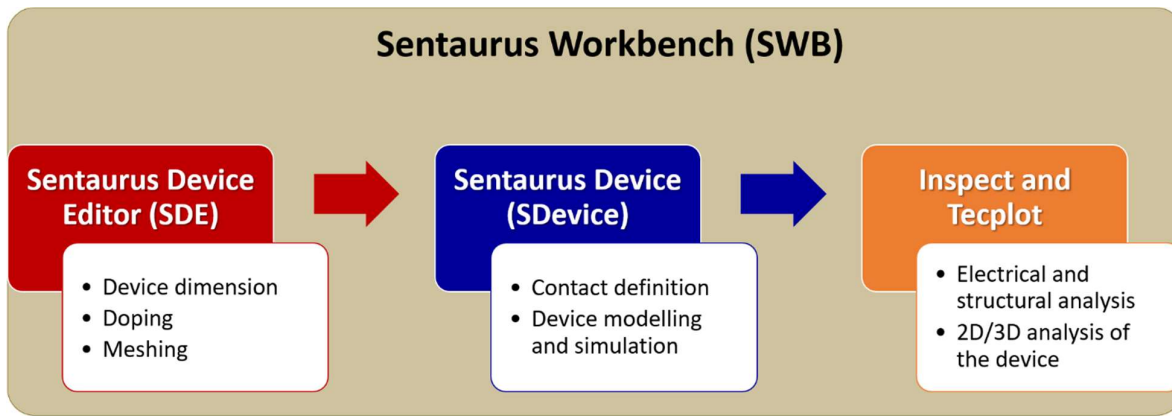
Figure 2.1: A generalized Sentaurus TCAD process flow utilized in this thesis.

2.1.2 Sentaurus Device Editor (SDE)

Sentaurus Device editor (SDE) is a tool that is evolved to define the structure of the device prior to simulation. In the SDE, a command-based input file or a script written by the user is utilized to define the device structure, different contact areas for source, drain and gate, doping concentration, and many more. There are two possible ways to make the device structure in the SDE; one is to use the GUI builder of SDE, and another one is direct. Based on the input file, the SDE tool makes the device structure. The script file contains several sections. At the beginning of the script file, the user can define variables, can be utilized anywhere in the input file. As explained above, the Sentaurus TCAD provides inherent flexibility where the user can freely define the device dimension and any physical property as a variable to perform the simulation sequentially for different values of a particular variable.

After this, the structure of the device is defined by utilizing different rectangles and other polygons of desired materials, with the corresponding naming of each region. The naming of each region is used later in the SDE input file as well as SDevice command files. Further, the desired doping may be defined. In this work, the high doping concentration of the donors is employed in a little area near the source and drain contacts of the device to define the metal region. The mesh density is a vital part of device simulation, which is defined at last in the script of SDE by the formation of windows in the different shapes such as rectangles, lines, and other polygons, and the mesh density is specified at the ends of the window. Mesh also splits the device structure into a series of discrete points where the physical equations of different models can be solved in the SDevice section.

Increasing mesh density has an advantage in the accuracy of the device simulation and also has a disadvantage in terms of simulation time. Hence, it is necessary to balance the necessity of accuracy and simulation time. In order to balance both of them, the regions that are important for the device operation perspective high mesh density is preferred, whereas the areas in the device of least interest such as bulk and the substrate region, the low mesh density, are preferred. The high mesh density region is usually the AlGaN/GaN heterointerface, the channel region, gate, drain, and source edges. Figure 2.2 shows the device structure designed in the SDE and corresponding meshing in the device. The epitaxial structure of the device on Si substrate was shown in Figure 2.2 (a), and the enlarged image is shown in Figure 2.2(b) illustrates the layers close to the surface and the drain region. After simulating the SDE, the structure with meshing has been depicted in Figure 2.2 (c). The x and y-axis shown in Figure 2.2 are in µm. The different colors in Figure 2.2 in the device explain the different materials where the pink, red, dark purple, and grey colors indicate the Silicon, AlN, AlGaN, and GaN, respectively, the light blue color in Figure 2.2 (b) specifies the ambient. Figure 2.2 (d) is the device schematic of the designed AlGaN/GaN HEMT, which depicts the thickness of each layer. Furthermore, the length of the device is 10 µm. The Gate to Source length (L_{GS}) is 1 µm, length of Gate (L_G) is 3 µm, and length

of Gate to Drain (L_{GD}) is 4 µm. Here, the device possesses high-density meshing at the source and drain edge and the 2DEG region, whereas the low density of meshing shows the area of least interest, as explained above. The total mesh density in the simulated devices was determined by the number of mesh points in the order of thousands, as calculated in the simulation. Usually, the optimal meshing also solves the convergence problem that occurred during the simulation.

(a)

(b)

(c)

(d)
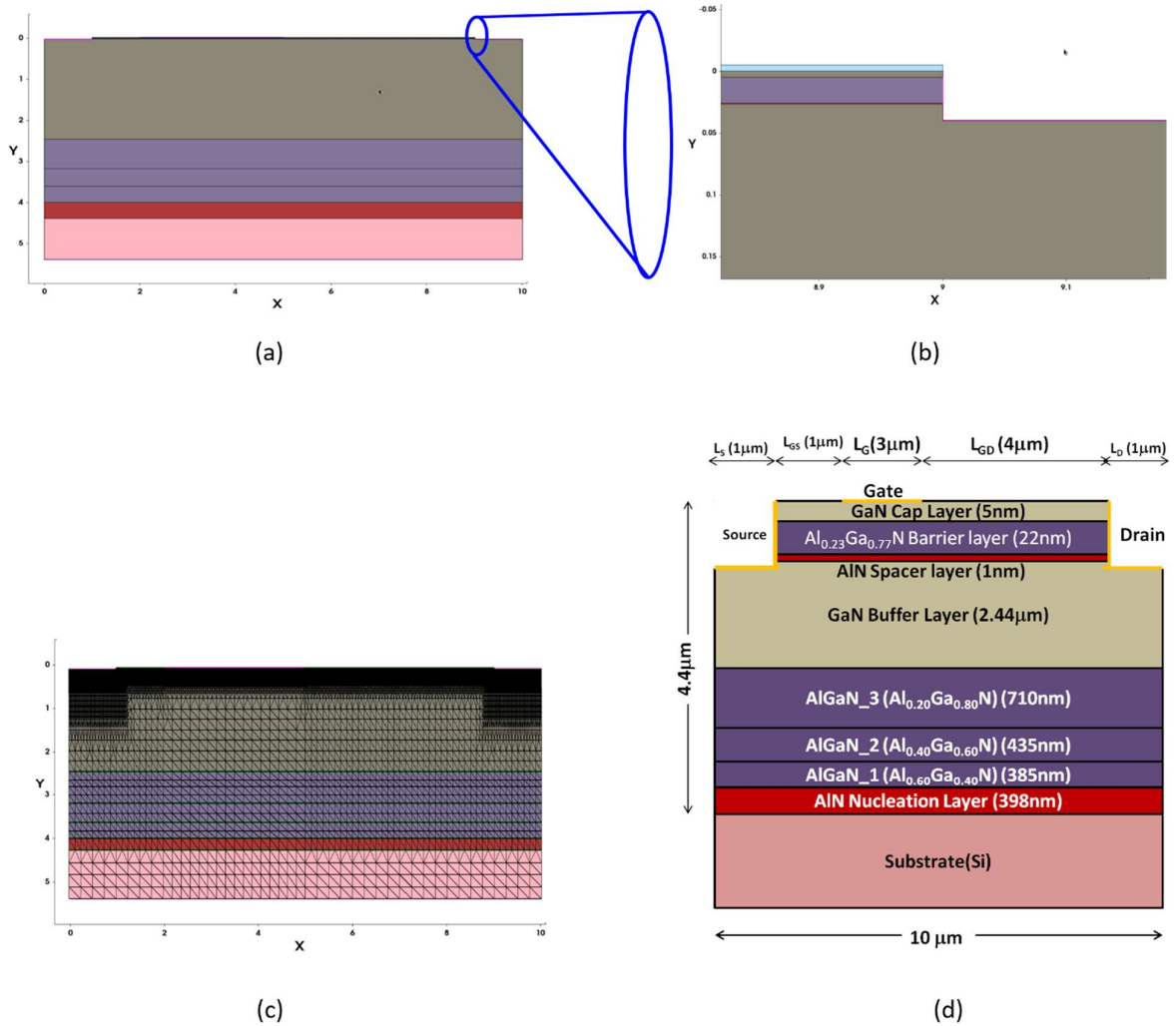
Figure 2.2: (a) The epitaxial structure of the designed AlGaN/GaN HEMT (b) Enlarged view of designed structure indicating top layers of the device (c) Optimal meshing of the designed AlGaN/GaN HEMT. (The X and Y-axis are in µm scale) (d) Schematic cross-section view of Designed AlGaN/GaN HEMT

2.1.3 Sentaurus Device (SDevice)

Sentaurus Device (SDevice) is a tool developed by synopsis to perform numerical simulation for different physical and mathematical models and associated material parameters described by the user in the command-based script file of the SDevice. There are two kinds of input files essential to perform the simulation using the SDevice tool. One is parameter files of desired materials where the standard values of the material parameters were defined; another one is the command-based script file, which calls the user-defined standard models and parameter files to perform the device simulation. The SDevice solves these equations, models, and parameters at each mesh point defined by the user in the SDE and performs desired DC, AC, and transient device simulations as defined by the user. Additionally, it also provides output files comprising information related to potential, charge densities, electric fields, mobility, polarization, energy bands, and temperature profile of the device after simulation.

SDevice provides the facility to the users to define a specific set of parameters in the script, which are desirable for the device simulation. A typical input command file of SDevice consists

33

of the following sections: *File, Electrode, Physics, Math, Plot,* and *Solve*. Each section of the SDevice is discussed as follows [Liddle, 2008; Sentaurus, 2013]:

(a) File Section

The file section is just like a recording section, which maintains track of all of the simulation files defined by the user in this section throughout the simulation. Moreover, it also defines the input and output files required to execute the device simulation.

(b) Electrode Section

The electrode section defines all of the contacts, including source, drain, and gate along with their type, i.e., *Ohmic* and *Schottky*, in the command section of SDevice utilized in the device simulations. The definition of these electrodes or contacts also utilizes electrical boundary conditions with no meshing conditions. In this work, the source and drain contacts are Ohmic, which is described in the electrode section along with their initial voltage condition, i.e., 0 V for all cases, and the series resistance or the contact resistance were also defined for the same. Since the gate contact in the designed AlGaN/GaN HEMT is Schottky contact and hence defined differently than the source and drain contacts, i.e., the metal work-function of the gate metal and the initial voltage with contact type (Schottky) is defined in this section [Liddle, 2008]. It is imperative to define all the contacts related to the device in this section because the contacts which are not defined as electrodes in this section are ignored by SDevice during the simulation.

(c) Physics Section

The physics section is one of the most important and relatively complicated section, which permits the selection of different physical models such as mobility, polarizations, tunneling, drift and diffusion, thermodynamic, and so on, required for the particular device simulation. The physics section contains two prominent ways to define these models: one is global, and another is the interface or region-specific physics. Global physics can be applied to the whole device, while region-specific physics can be implemented in particular regions and interfaces[Liddle, 2008]. The detailed description related to physical models utilized in the AlGaN/GaN HEMT device simulation is described in section 2.9.

(d) Math Section

In this section, the *SDevice* solves the partial differential equations relevant to the device at each mesh point, iteratively and self-consistently. In each iteration, the calculation of error is performed, and the SDevice goes to converge the solution that touches the error, having a lower threshold defined by the user. The maximum number of iterations performed for each step at each mesh point before a solution is reached. If the solver does not obtain the solution in the defined error-threshold, the *SDevice* reduces the step size automatically and starts fresh iteration until it achieves the error threshold or the minimum step size defined by the user in the *Solve* section. Moreover, the math block also contains different mathematical constraints for the numeric solver.

(e) Plot Section

The Plot section specifies the calculated quantities and solution variables throughout the simulation. It also saved the simulated data to the output plot files in *.plt* and *.tdr* format. In the plot file, the data computed by SDevice based on the selected physics models is saved [Sentaurus, 2013].

(f) Solve section

The Solve section defines the desired set of equations to be solved during simulations. In general, the equations utilized for device simulation by the solve section are Poisson's equation, and the electron and hole current continuity equation will be explained in the next section. The solve section mainly determined the solution of the electric fields in the designed devices, and hence both of these equations need to be solved. Additionally, the solve section starts calculation

by keeping all the contacts at zero potential and increase it to the user-specified conditions and observe the solutions at different mesh points by considering the step size for each iteration as described in the math section.

2.1.4 Inspect and Tecplot

The *Inspect* and *Tecplot* are the tools employed to imagine the device corresponding simulated results, including I-V characteristics, electron and hole density, energy levels, carrier concertation, and many more. In addition, the output characteristics of the device, e.g., electric field, electrostatic potential, and many more, can be inspected. The diagrams obtained from Tecplot will be involved in this chapter, which can provide the pictorial representation of the device operation. By utilizing these diagrams, the data can be extracted by putting horizontal and vertical lines, which can provide more information about the device and can be used in further analysis.

2.2 PHYSICAL MODELS AND EQUATIONS

The Sentaurus TCAD provides several physical models to explain the device physics for the designed device to observe the results similar to the real device. These physical models explain the behavior of the charge carriers along with various boundary conditions like the electric field, lattice temperature, electrostatic potential, bandgap variation, and quantum effects. Depending upon the device types and their operating conditions, the user needs to include the corresponding physical models to perform simulations to observe estimations about the device characteristics and behavior. In this section, different physical models utilized in this thesis are presented and discussed briefly.

In order to explain the charge transport phenomenon in the device, the fundamental equations that manage the transport of carriers are Poisson's equation and the continuity equation. The Poisson's equation calculates self-consistent electrostatic potential through the hole and electron concentrations and the electron and hole continuity equations calculation of current. In order to determine the self-consistent solution, it is essential to calculate the current densities, J_n, and J_p, from the electrostatic potential and the carrier concentrations, which is realized by using the charge transport models. In this work, the following equations and models were incorporated in the *SDevice* to perform the simulation.

2.2.1 Charge Transport Equations

The charge transport in a semiconductor in the presence of an electric field is described by the self-consistent solution of the Poisson and the current continuity equations for the electrons and holes.

The TCAD simulation solves three fundamental equations of the semiconductor devices, namely the Poisson equation and electron and hole continuity equations. These equations analyze the electrical characteristics of the device. The self-consistent solution of these equations defines the charge transport in the presence of an electric field in a device. The Poisson's equation determines the correlation between electrostatic potential, *f* to the given charge distribution and can be given as [Sentaurus, 2013]:

$$\nabla.(\varepsilon.\nabla\phi) = -q(p - n + N_D - N_A) - \rho_{trap} \tag{2.1}$$

where ε is the electrical permittivity, q electronic charge, n electron density, p hole density (for AlGaN/GaN HEMT, it is $\approx$ 0), N_D ionized donor concentration, N_A ionized acceptor concentration, ρ_{trap} charge density contributed by traps, ϕ electrostatic potential.

The charge carrier transport in a semiconductor device needs to be considered for device modeling and simulation. The SDevice also provides the platform for many charge-transport

models, which can be utilized for different semiconductors. These models can be represented in the form of continuity equations. The continuity equations define charge conservation as:

$$\nabla.\vec{J_n} = qR_{net} + q\frac{\partial n}{\partial t} \tag{2.2}$$

$$-\nabla.\vec{J_p} = qR_{net} + q\frac{\partial p}{\partial t} \tag{2.3}$$

where $\vec{J_n}$ and $\vec{J_p}$ are the electron and hole current density, respectively, and R_{net} is the net recombination rate.

2.2.2 Drift-Diffusion Model

The default carrier transport model used by the SDevice is *the Drift-Diffusion* model. It employs the approximations in the *Boltzmann Transport Equations*, where the flow of charge carriers in the device is due to their drift and diffusion in the presence of an external electric field along with their generation and recombination. The electric field provides the directed motion to the charge carriers. While the current is the flow of charge carriers, i.e., electrons and holes, therefore the current density for the electrons and holes can be given as [Balaz, 2011]:

$$\vec{J}_{Drift} = q(n\mu_n + p\mu_p)\vec{E} \tag{2.4}$$

where μ_p and μ_n indicates the mobilities of holes and electrons, respectively.

Diffusion is a process in which the particles move from the high concentration region to the low concentration region due to random thermal motion [Balaz, 2011; Sze and Lee, 2012]. The diffusion flux or flow of charge carrier is, therefore, directly proportional to the concentration gradient. The flow of carriers or the flux of the carriers is termed as diffusion current and can be given as [Sze and Lee, 2012]:

$$\vec{J_n} = qD_n\frac{d\Delta n}{dx} \tag{2.5}$$

$$\vec{J_p} = -qD_p\frac{d\Delta p}{dx} \tag{2.6}$$

where D_n and D_p are proportionality constants termed as diffusion constants or diffusivity. Using the Einstein relationship, the diffusivities D_n and D_p can be specified by their mobilities as [Sze and Lee, 2012]:

$$D_n = \left(\frac{kT}{q}\right)\mu_n \tag{2.7}$$

$$D_p = \left(\frac{kT}{q}\right)\mu_p \tag{2.8}$$

The Einstein relationship connects the drift and diffusion current expressions as they have the same quantities except for the multiplication coefficient. Hence, by utilizing the Einstein relationship into the drift and diffusion current, the combined drift and diffusion current expression can be given as:

$$\vec{J_n} = -qn\mu_n\nabla\phi_n \tag{2.9}$$

$$\vec{J_p} = -qp\mu_p\nabla\phi_p \tag{2.10}$$

where ϕ_p and ϕ_n are the quasi-Fermi potentials for holes and electrons, respectively. This drift-diffusion model can be used to solve the lattice temperature equation.

2.2.3 Thermodynamic Model

The *Thermodynamic* model is generalized as an extension of the drift-diffusion model along with the incorporation of temperature gradients in the drift-diffusion equations of the device. It solves the equations of the lattice temperature along with the continuity equations. In the case of high-power applications for AlGaN/GaN HEMT, the current and voltage levels are very high and generate much heat during the operation and hence the calculation of the device temperature and the corresponding impact on device behavior is very important. Thus, the temperature-dependent calculation of the AlGaN/GaN HEMT can be performed by this model. The thermodynamic model can be signified in Sentaurus TCAD as [Sentaurus, 2013]:

$$\vec{J_n} = -qn\mu_n(\nabla\phi_n + P_n\nabla T) \tag{2.11}$$

$$\vec{J_p} = -qp\mu_p(\nabla\phi_p + P_p\nabla T) \tag{2.12}$$

where P_p and P_n are the absolute hole and electron thermoelectric powers, respectively, and T is the lattice temperature. The AlGaN/GaN HEMT conceded self-heating; thus, for the accurate simulation of self-heating effects, this extra driving force for the current can be included by specifying the Thermodynamic keyword in the Sentaurus TCAD physics section. By considering the self-heating phenomenon, *Thermodes* are defined with heat fluxes by specifying Temperature and *SurfaceResistance* in the thermode/electrode section.

2.2.4 Mobility Model

SDevice utilizes a modular process for the explanation of the carrier mobilities. Mobility is a measure of the collective response of the carriers to the electric field *E*. The mobility can be determined by employing several scattering mechanisms, e.g., phonon, carrier, ionized impurities, surface roughness, and other types of scattering. In a simple way, mobility is a function of the lattice temperature and is described in the constant mobility model in the SDevice, which occurs because of Phonon Scattering. This constant mobility model should be used only for undoped materials [Sentaurus, 2013]. Sentaurus TCAD provides a variety of models in the SDevice that can be employed in doped and semiconductors for device modeling and simulation applications. These are Philips Unified Mobility Model, Masetti model, Arora model, Lombardi model, University of Bologna Model, and many more. All these models were utilized for different scattering and doping mechanism, e.g., Philips Unified Mobility Model is employed for both impurity and carrier scattering phenomenon; the Masetti model is calibrated for the simulation of doping-dependent mobility in silicon and so on [Sentaurus, 2013]. There are two mobility models were utilized in this work for the low field and high field mobility analysis are [Nigam *et al.*, 2017]:

(a) Arora model
(b) Transfer electron effect-2 model

(a) Arora Model

The temperature-dependent mobility can be observed either from Monte-Carlo (MC) simulation or the utilization of experimental data to fit the well-known Arora model in the SDevice. Thus, the Arora model has been employed here for the low field as well as temperature depended on mobility analysis for both electrons and holes in the designed AlGaN/GaN HEMT by simulation and can be given as [Arora *et al.*, 1982; Nigam *et al.*, 2017; Sabui *et al.*, 2016]:

$$\mu = \mu_{min} + \frac{\mu_d}{1 + \left(\frac{N_{tot}}{N_0}\right)^{A^*}} \tag{2.13}$$

where the parameters μ_{min}, μ_d, N_0, and A^* can be determined as:

$$\mu_{min} = A_{min}\left(\frac{T}{300K}\right)^{\alpha_m} \tag{2.14}$$

$$\mu_d = A_d\left(\frac{T}{300K}\right)^{\alpha_d} \tag{2.15}$$

$$N_0 = A_N\left(\frac{T}{300K}\right)^{\alpha_N} \tag{2.16}$$

$$A^* = A_a\left(\frac{T}{300K}\right)^{\alpha_a} \tag{2.17}$$

where μ_{min} is minimum mobility and A_{min}, A_{max}, α_a, A_a, A_N, α_N, α_d, α_m are the fitting parameters. The A_{max} has been calibrated for the device's low field mobility for the best fit of mobility. Since the Arora model is defined for InN in Sentaurus, TCAD parameters fail and require calibration. Thus, the parameter values are modified with the GaN parameters [Nigam *et al.*, 2017; Piprek, 2007; Sentaurus, 2013]. These parameters are calibrated for our model, and these are shown in Table 2.1. The mobility μ is used in the electron and hole continuity equations.

Table 2.1: Parameters of Arora Model for GaN [Nigam *et al.*, 2017]

Symbol	Electrons	Holes	Units
A_{min}	88	54.3	$cm^2V^{-1}.s^{-1}$
α_m	-6.70×10^{-1}	-5.70×10^{-1}	
A_d	1720	470	$cm^2V^{-1}.s^{-1}$
α_d	-4.00	-2.23	
A_N	1.25×10^{17}	2.35×10^{17}	cm^{-3}
α_N	1.9	2.4	
A_a	9.8×10^{-1}	8.8×10^{-1}	
α_a	-1.50×10^{-1}	-1.46×10^{-1}	

(b)Transferred Electron Effect-2 Model

At high electric fields, negative differential mobility was usually seen in the GaN and other III-N materials and devices. This effect occurs due to electron transfer into a high energic valley with a much greater effective mass. In order to observed this effect, Sentaurus includes a transferred electron effect model-2 (the transferred electron effect model is defined for GaAs and family) in the SDevice and also was included and modeled in our work by the following equation [Nigam *et al.*, 2017; Sabui *et al.*, 2016; Sentaurus, 2013]:

$$\mu = \frac{\mu_{low} + \mu_1\left(\frac{F_{hfs}}{E_0}\right)^{\alpha} + v_{sat}\frac{F_{hfs}^{\beta-1}}{E_1^{\beta}}}{1 + \gamma\left(\frac{F_{hfs}}{E_0}\right)^{\alpha} + \left(\frac{F_{hfs}}{E_1}\right)^{\beta}} \tag{2.18}$$

The transferred electron effect-2 model comes into effect when maximum drift velocity has been reached at the particular electric field. Here μ_{low} is low field mobility, and E is the electric field. The E_c, F_{hfs}, v_{sat}, α, β and γ are the fitting parameters [Sabui *et al.*, 2016; Sentaurus, 2013]. The default parameters of the transferred electron effect-2 model used by Sentaurus SDevice for $Al_xGa_{1-x}N$ are specified in Table 2.2.

Table 2.2: Parameters of Transferred electron effect-2 model for $Al_xGa_{1-x}N$ [Sentaurus, 2013].

Material	α	β	γ	$E_0 = E_1$ [V.cm^{-1}]	μ_1 [cm^2.V^{-1}.s^{-1}]
AlN	0.8554	17.3681	8.7253	447033.9	0
Al$_{0.8}$Ga$_{0.2}$N	0.8324	12.5795	8.6037	386244.0	0
Al$_{0.5}$Ga$_{0.5}$N	0.8080	9.4438	8.0022	304554.1	0
Al$_{0.2}$Ga$_{0.8}$N	0.7897	7.8138	6.9502	245579.4	0
GaN	0.7857	7.2044	6.1973	220893.6	0

2.2.5 Bandgap Model

The bandgap is the energy difference between the highest energy in the valance band and the lowest energy in the conduction band. The electron affinity is the difference between the vacuum level and the lowest energy in the conduction band. The SDevice offers various bandgap models such as BennettWilson, Varshni, delAlamo, OldSlotboom, JainRoulston, and many more [Sentaurus, 2013]. Depending on material and device properties, a suitable model can be preferred in the simulation. In this work, Varshni expression [Nigam *et al.*, 2017; Varshni, 1967] is used to calculate bandgap in AlGaN/GaN HEMT, which explains the temperature dependence of the bandgap. The expression of Varshni model is given as:

$$E(T) = E_g(0) - \frac{\alpha T^2}{T + \beta} \tag{2.19}$$

where $E_g(0)$ is the bandgap of GaN at 0 K temperature; α is empirical constant, and β is the constant associated with Debye temperature. The values of $E_g(0)$, α and β are 3.47 eV, 7.40×10^{-4} eV.K^{-1}, and 600 K extracted respectively.

2.2.6 Tunneling Model

The tunneling is a significant and crucial physical effect that occurs in micro and nanoelectronic devices. Depending upon the devices, the tunneling phenomenon can be advantageous or problematic. In small-scale devices such as MOSFETs and HEMTs, tunneling causes undesired leakage currents near the gate region. However, tunneling is necessary for other devices such as EEPROMs for the device operation. In order to consider the tunneling effects in the device, the Sentaurus TCAD provides 3 tunneling models:

(a) Direct tunneling model
(b) Fowler-Nordheim (FN) tunneling model
(c) Nonlocal tunneling model

(a) Direct Tunneling Model

The direct tunneling model presumes a trapezoidal barrier and ignores the heating of the tunneling carriers. This model has been used to describe leakage through thin gate insulators, provided those are of uniform or uniformly graded composition.

(b) Fowler-Nordheim Tunneling Model

Fowler–Nordheim tunneling is the simplest tunneling model. It is a particular case of tunneling also covered by the nonlocal and direct tunneling models, where tunneling is to the conduction band of the oxide.

(c) Nonlocal (NLM) Tunneling Model

The nonlocal mesh tunneling model is the most versatile tunneling model that handles arbitrary barrier shapes, includes carrier heating terms, and offers several different estimations for tunneling probability. This model is defined to describe tunneling at Schottky contacts, tunneling at heterostructures, and gate leakage through thin stacked insulators. Thus, as per the

above explanation, the nonlocal mesh tunneling model can be employed for simulation of the AlGaN/GaN HEMT [Sentaurus, 2013] and used in the device simulation in the present work. This model is defined in the TCAD simulator to describe tunneling at heterostructures, at Schottky contacts, and gate leakage through thin insulator stacks. In order to utilize the NLM tunneling model, a nonlocal mesh near the gate of the AlGaN/GaN HEMT was constructed. Subsequently, the physical details of the NLM tunneling model have been specified in the command section of the SDevice; after that, the NLM tunneling model parameters have been defined in the parameter file. Moreover, the nonlocal mesh length was also defined in the Math section of the device, and it has been optimized as 15 nm [Nigam *et al.*, 2017]. The detailed description regarding the NLM tunneling model has been explained in the SDevice user guide of the Sentaurus TCAD [Sentaurus, 2013].

For our device, the tunneling probability of 0.22 is calibrated by simulation. The tunneling is not only due to Schottky contact or heterointerface but also the surface states or traps available at the top of the device. Thus, surface traps energy levels also affect the off current of the device. Generally, surface traps are donor level traps formed due to the availability of dangling bonds at the surface. The combined effect of tunneling probability and traps gives the OFF current [Nigam *et al.*, 2017].

2.2.7 Generation and Recombination Model

Generation and recombination are very important processes for charge carrier exchange carriers between the valence and the conduction band. As explained in section 1.3.4 of chapter 1, in the AlGaN/GaN HEMT, some allowed energy states called traps are present in the forbidden energy level. These traps behave as recombination centers and can cause a significant impact on the device operation. Hence, to observe the impact of these charges, some fixed interface charges, bulk and surface traps were introduced in the device analysis. In our simulation, Shockley-Read-Hall (SRH) recombination was used to calculate dynamic traps in the device [Miccoli *et al.*, 2013; Nigam *et al.*, 2017]. It also assumes that there are traps that exist at a particular energy level within the bandgap. In our device simulation, Sentaurus uses the following set of equations [Sentaurus, 2013]:

$$R_{net}^{SRH} = \frac{np - n_{i,eff}^2}{\tau_p(n + n_1) + \tau_n(p + p_1)} \tag{2.20}$$

with

$$n_1 = n_{i,eff} \, exp\left(\frac{E_{trap}}{kT}\right) \tag{2.21}$$

$$p_1 = n_{i,eff} \, exp\left(\frac{E_{trap}}{kT}\right) \tag{2.22}$$

where E_{trap} is the difference between the defect level and the intrinsic level. The τ_n and τ_p are carrier lifetime, modeled as a product of a doping-dependent, field-dependent, and temperature-dependent factor:

$$\tau_C = \tau_{dop} \frac{f(T)}{1 + g_C(F)} \tag{2.23}$$

where $c = n$ and $c = p$ for electrons and holes, respectively. Since the donor level traps are presented at the surface of the device, therefore the concentration of these traps have been optimized as 2×10^{13} cm^{-2} with the energy level 0.15 *eV* below from the conduction band by simulation [Nigam *et al.*, 2017]. The electron and hole capture cross-section for interface traps is about 1×10^{15} cm^{-2} observed by the simulation [Miccoli *et al.*, 2013].

2.2.8 Polarization Model

Sentaurus TCAD provides the facility to analyze the piezoelectric polarization in the III-Ns by the stress and strain models. The polarization in III-N is already explained in section 1.1.2 of chapter-1 in detail. The piezoelectric polarization effect provides information about charges at the AlGaN/GaN heterointerface and forms 2DEG. Thus, polarization induced sheet carrier concentration at the $Al_{0.23}Ga_{0.77}N/GaN$ is calculated by the piezoelectric polarization model suggested by Ambacher *et al.* [Ambacher *et al.*, 1999a; Ambacher *et al.*, 2002]. The following equation calculates the piezoelectric polarization:

$$P_z^{pz} = 2d_{31}\sigma_1 = 2d_{31}\varepsilon_1 \left(c_{11} + c_{12} - 2\frac{c_{13}^2}{c_{33}} \right) \tag{2.24}$$

where d_{31} is piezoelectric coefficients (cm/V), c_{11}, c_{12}, c_{13} and c_{33} are stiffness constants (Pa), and ε_1 is strain coefficient. P_z^{pz} is piezoelectric polarization in the z-direction, which is only one nonvanishing component directed towards the growth direction, as explained in section 1.1.2. The piezoelectric charge is computed in simulation according to the following equation [Sentaurus, 2013]:

$$q_{PE} = -activation \ \nabla.P_z^{pz} \tag{2.25}$$

where *activation* is a calibration parameter whose value is calibrated as ~0.38 in simulation [Nigam *et al.*, 2017]. The q_{PE} value is added to the Poisson's equation [Sentaurus, 2013], which significantly affect the device threshold voltage and can be given as:

$$\nabla.(\epsilon\nabla\phi) = -q(p - n + N_D - N_A + q_{PE}) \tag{2.26}$$

2.3 VALIDATION OF SIMULATED RESULTS WITH EXPERIMENTAL RESULTS AND EFFECT OF SELF-HEATING ON ELECTRICAL CHARACTERISTICS OF AlGaN/GaN HEMT

In this work, the structure of AlGaN/GaN HEMT has grown on Si (111) substrate. As explained previously, the utilization of Si substrate for the fabrication of AlGaN/GaN HEMT is very advantageous in terms of availability of the substrate and the integration possibilities with the well matured Si industry. Additionally, Different orientations of Si were studied for GaN HEMT by various research groups to investigate efficient power device platforms. Boulay *et al.* demonstrated GaN HEMTs on (001) oriented Si substrate for microwave power application [Boulay *et al.*, 2007]. The Si (001) possesses four-fold symmetry that is suitable for the growth of the cubic phase, but the Si (111) provides a hexagonal symmetry surface which is more suitable for epitaxial growth of the wurtzite phase [Bhat *et al.*, 2011]. This work has been carried out in collaboration with A*STAR, Singapore, for experimental analysis, in which the AlGaN/GaN HEMT has been fabricated on Si (111) substrate by MOCVD. The details of the epitaxial growth of AlGaN/GaN HEMT and growth parameters utilized in the simulation work were explained by Bhat *et al.* in his report [Bhat et al., 2014] and shown in Figure 2.2(d).

### 2.3.1 Simulation Results and Experimental Validation

The validation of the device structure has been done by comparing simulated DC transfer characteristics to experimental transfer characteristics of HEMT, as shown in Figure 2.3. The plots show good agreement between simulated and experimental transfer characteristics of the device with applied gate bias at a drain voltage of 10 V. The gate bias has been varied from the pinched-off region to the ON state region (between -5 V to 2 V). The transconductance characteristics of simulated and experimental results also have been shown in Figure 2.3. An increment of transconductance above V_{GS}= - 2V in transconductance (g_m) versus gate voltage (V_{GS}) is clearly seen. These characteristics explain that the channel is completely off at lower gate voltage (V_{GS} <
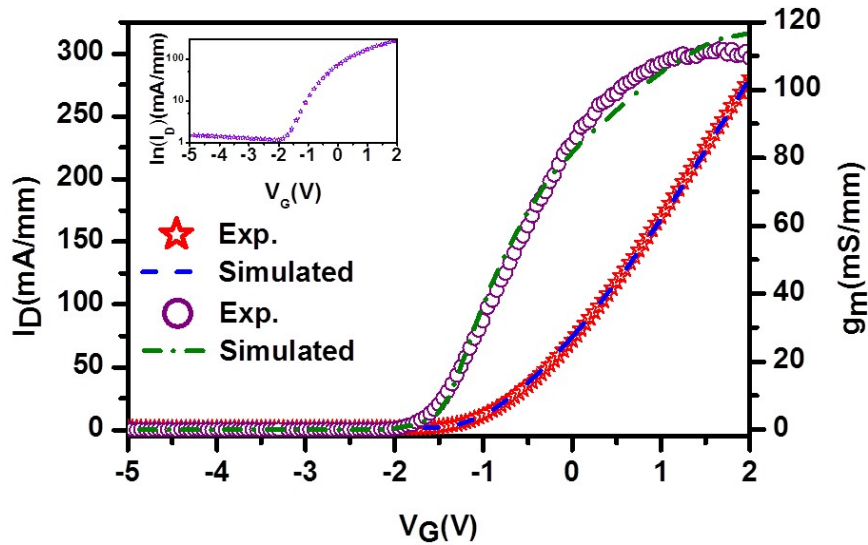
Figure 2.3: Experimental (star symbol) and Simulated (dashed line) Drain current vs. Gate voltage (I_D-V_G) characteristics of HEMT at V_D=10 V along with Transconductance (g_m) with experimental (purple circle symbol) and simulated curve (dash-dot line) at V_D=10 V and 300 K. Logarithmic transfer characteristics of HEMT shown in inset.

-2V). When the gate voltage increases above pinched off region, the channel gradually starts forming, and hence, channel resistance starts dominating in the ON state [Nigam *et al.*, 2017].

It can be seen that the transconductance starts saturating at a higher gate voltage. The maximum transconductance has been obtained by simulation as 116.8 mS/mm at 300 K, which shows good agreement with the experimental data, 115 ± 10 mS/mm at 300 K, as shown in Figure 2.3. The contact resistance for the device is being calculated as 0.2 Ω.mm by simulation, and the initial sheet carrier concentration is calculated as 3.7×10^{12} cm^{-2} at the interface. Due to the triangular quantum well at AlGaN/GaN heterointerface in the conduction band, the electrons confine and 2DEG forms. The band diagram of the simulated structure has shown in Figure 2.4. The band diagram and 2DEG were observed at the initialization of the device simulation, i.e., when no external bias was applied (V_{GS}= 0 V and V_{DS}= 0 V). In this condition, the electron density at 2DEG is 2×10^{19} cm^{-3}, which provides a channel for transmission of charge carriers for device operation [Nigam *et al.*, 2017].
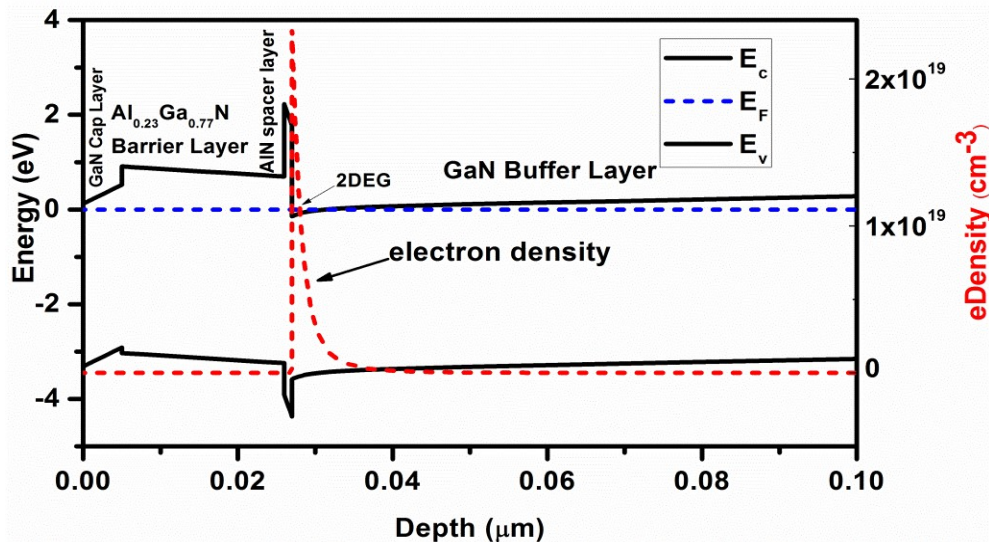
Figure 2.4: Band diagram of the top layers of AlGaN/GaN HEMT and electron density at the 2DEG interface.

Further, the 2DEG electron density and sheet carrier concentration were also measured under external biasing conditions by applying V_{DS} =10 V, and V_{GS} = 0 V. Figure 2.2 (b) shows the 2DEG electron density at V_{DS} =10V and V_{GS} = 0 V. Here, the 2DEG electron density was observed as 7.2×10^{19} cm^{-3} and 2DEG concertation was obtained as 1.06×10^{13} cm^{-2}. Moreover, the Hall measurements were performed to obtain 2DEG carrier concentration, where the 2DEG carrier concentration was measured as 1.1×10^{13} cm^{-2}. This value is close to the observed 2DEG concentration by simulation [Bhat et al., 2014; Nigam et al., 2017].

Moreover, the piezoelectric polarization is also observed in the device by utilizing the polarization model described in previous sections and has been shown in Figure 2.5 (a). It has been observed that the incorporation of a thin AlN spacer layer at the AlGaN/GaN heterointerface provides more strain and provides more piezoelectric polarization at 2DEG, which in turn increases the electron density at the 2DEG. There is an intentional background carbon doping due to low pressure tuning at the interface of GaN/Al$_{0.2}$Ga$_{0.8}$N. Since carbon is a very effective acceptor; thus, it creates acceptor type traps in bulk. In order to define carbon doping, an analytical doping profile has been created at the interface of GaN/Al$_{0.2}$Ga$_{0.8}$N, which shows the diffusion of carbon towards GaN. The carbon doping is considered as acceptor type buffer traps. The concentration of these buffer traps is optimized by simulation as 1×10^{15} cm^{-3} with the energy level of E$_C$-0.25 eV [Nigam et al., 2017].
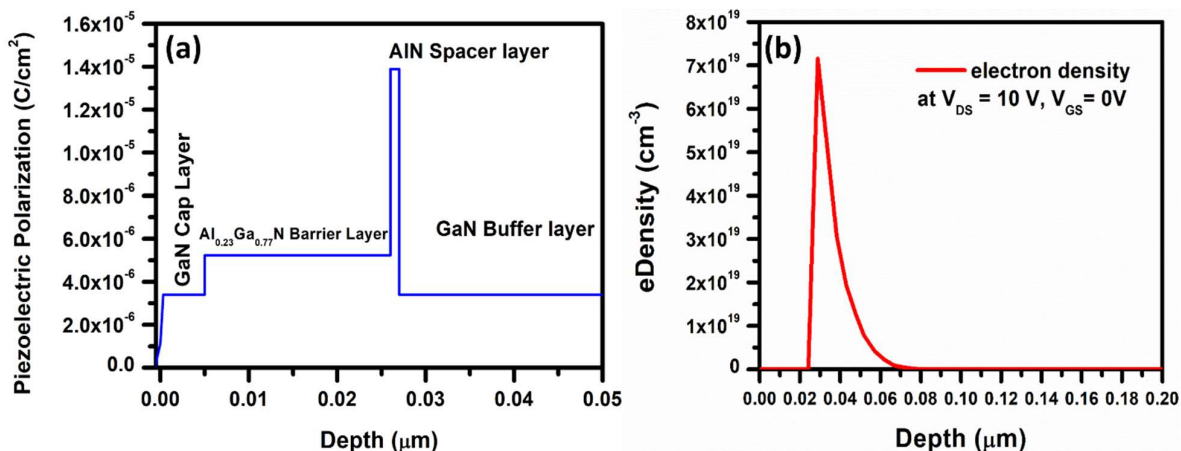
Figure 2.5: (a) Observation of piezoelectric polarization at the top layers of the designed AlGaN/GaN HEMT (b) 2DEG electron density at AlGaN/GaN heterojunction at V_{DS}=10 V and V_{GS}=0 V

2.3.2 Impact of Self-Heating Effect on The Electrical Characteristics of AlGaN/GaN HEMT

The self-heating effects are considered by calculating lattice heat equations, which are taken into account by using the thermodynamic transport model [Sentaurus, 2013]. In this model, the drift-diffusion equations are extended to accounting electro-thermal effects. Initially, the charge carriers are in thermal equilibrium in the lattice. Hence, in this model, the charge carriers and lattice temperature are described by the single temperature. A set of equations, namely Poisson, electron and hole continuity equations, and lattice heat flow equations, are solved in simulation. For the solution of the equations for self-hating, some thermal boundaries also have been applied. In the AlGaN/GaN HEMT shown in Figure 2.2, there is an uninterrupted growth of the GaN layer without any interlayer [Bhat et al., 2014]. Thus, the heat flow is considered from the active layers of the HEMT to the Si substrate [Nigam et al., 2017]. For this, the thermal resistance can be calculated as [Cheng et al., 2010]:

$$R_{TH} = \frac{1}{\pi k_{Si}} \ln\left(\frac{8 t_{Si}}{\pi L_G}\right) \tag{2.27}$$

where t_{Si} is substrate thickness, L_G is gate length, k is thermal conductivity. Where the thermal conductivity of silicon is given by [Chattopadhyaya and Tokekar, 2008]:

$$k_{Si} = 1.57 \left(\frac{T}{300}\right)^{-1.4} \tag{2.28}$$

The thermal resistance can relate to the effective channel temperature and power dissipated, which is given as [Cheng *et al.*, 2010]:

$$P_{diss} = \frac{T_{eff} - T_{sub}}{R_{TH}} \tag{2.29}$$

where T_{sub} is the substrate temperature. The dissipated power can also be calculated by the sum of all terminal currents multiplied by their voltages, respectively. It can be given as [Sentaurus, 2013]:

$$P_{diss} = \sum IV \tag{2.30}$$
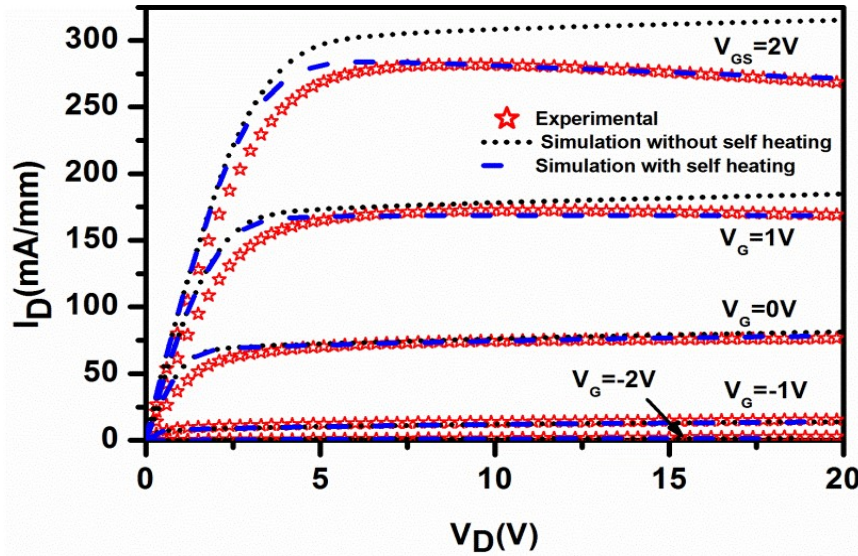
Figure 2.6: Variation of Drain current (I_D) and Drain voltage (V_D) for the HEMT with and without consideration of self-heating effects along with experimental results. A star symbol shows experimental results; dashed lines indicate simulated results with self-heating effects, and dotted lines show simulated results without self-heating effects.

Since the thermal impact of the substrate is considered as boundary conditions; thus, a thermode was inserted at the interface of AlN and Si substrate to extract the value of TBR (thermal boundary resistance). Several simulations have been carried out, and the value of TBR has been calibrated as 1×10^{-4} W^{-1}.cm^2.K. After the solution of the equations, thermal resistance has been obtained, 5.35 K.mm.W^{-1} and power has been calculated as 2.8 W/mm. at $V_{GS} = 2$ V and $V_{DS} = 10$ V [Nigam *et al.*, 2017].

Figure 2.6 shows the I_D-V_D characteristics of the device at different V_{GS}. Here V_{GS} is varied from -2 V to 2 V in the step of 1 V. The plots show transistors with good pinch-off characteristics. Dotted lines prescribe I-V characteristics of the device when the effects of self-heating are not considered. In this case, a significant deviation has been observed between experimental and simulated results. After the consideration of the self-heating effect, the results were shown in the figure by dashed lines. Moreover, the simulated I-V characteristics and experimental I-V characteristics are also matched. It can be seen in Figure 2.6 that at higher gate voltages, the saturation current decreases as drain voltage increases.
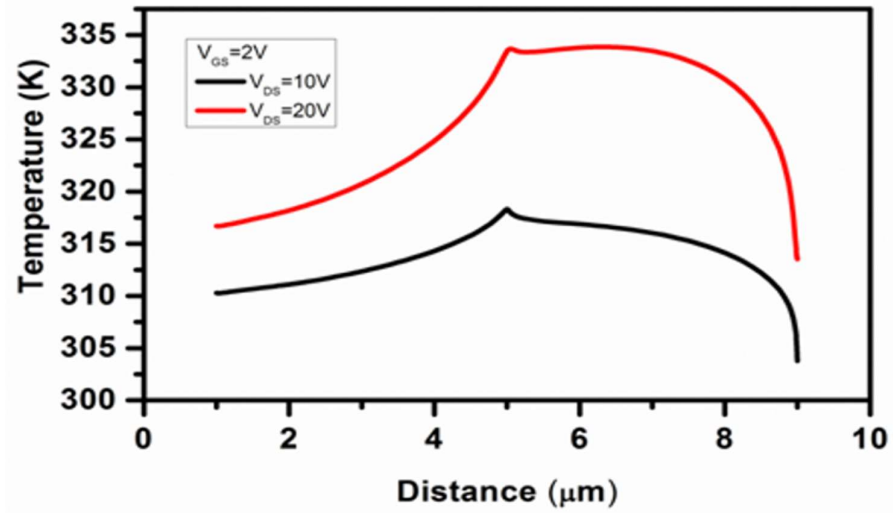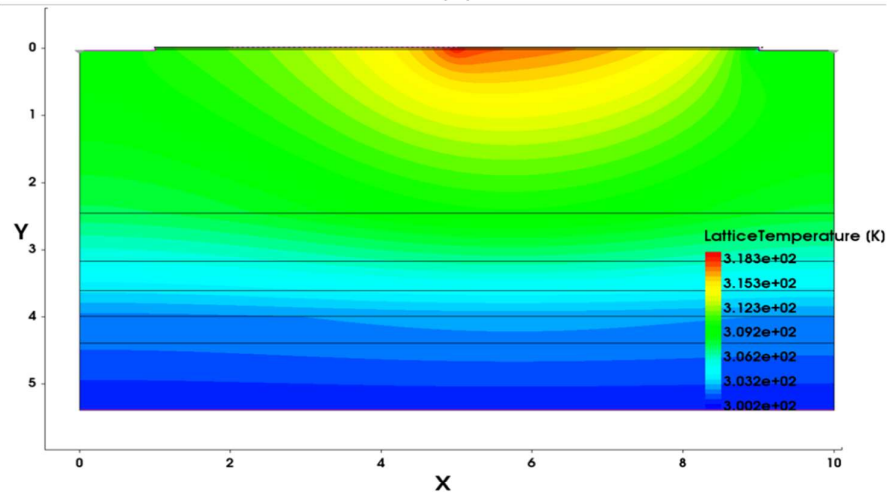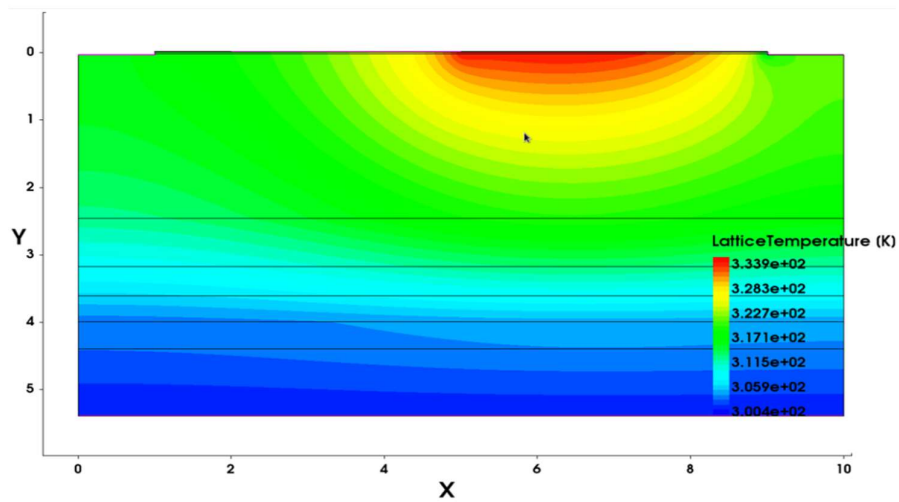
Figure 2.7: (a)Effects of self-heating at the 2DEG channel at V_{GS}= 2 V, V_{DS}=10 V, and 20 V from source to drain of the HEMT structure. (b)increment of lattice heat between drain and gate region at V_{GS}= 2 V, and V_{DS}=10 V and (c) V_{GS}= 2 V, and V_{DS}=20 V (x and y-axis are in μm range).

The self-heating has been observed at the gate edge between gate and drain. In this simulation, the temperature analysis for the self-heating effect has been done by consideration of two temperature profile on the same device at different drain voltages (V_{DS}=10 V and V_{DS}=20 V) with V_{GS} = 2 V. A peak of the temperature of 333 K and 318 K has been observed at the gate edge between the gate and drain at V_{DS} = 20 V and 10 V respectively as shown in Figure 2.7 (a) [Nigam *et al.*, 2017]. The channel temperature is low at lower V_{DS} due to low power dissipation and increased by a continuous increment in V_{DS}. Figure 2.7 (b) and Figure 2.7 (c) show a pictorial representation of the increment of lattice temperature in the device. It shows that as the drain V_{DS} increases, the I_{DS} increase, and the electric field between the drain and gate also increases. This increment in the electric field and high drain current causes the high phonon-phonon interaction in the 2DEG, which causes the increment of heat in the region, ultimately increases the lattice temperature.

2.4 SURFACE MODELING OF AlGaN/GaN HEMT FOR ION SENSING APPLICATIONS

When the surface of the gate region of the AlGaN/GaN HEMT is exposed to an aqueous solution of the heavy metal ions with a certain concentration, the variation in the surface charges and potential modulate the 2DEG charge density and hence the drain current changes. This mechanism can be employed to develop an ion sensor to measure the heavy metal ions in an aqueous solution. Commonly, when a solid surface (here gate region) is exposed in an ionic solution, the ions interact with the surface. This interaction forms an adsorption layer with surface charges on the solid surface [Rabbaa and Stiens, 2012]. As per the fundamentals of electrostatic physics, the developed surface charges due to the surface reactions produce an electric field, which changes the surface potential (ϕ_S) [van Hal *et al.*, 1996]. The layer of surface charges and counter-ions is also known as the electric double layer (EDL). The electric double layer might be divided into two different zones, a Helmholtz model and a Gouy-Chapman model and then combined after the Stern modification called the Gouy-Chapman-Stern model. It provides a more accurate illustration of the EDL model [Oldham, 2008]. Figure 2.8 depicts the schematic illustration of the Gouy-Chapman-Stern model. Here, the inner layer is closed to the solid surface, also known as the *compact layer* or *Helmholtz layer*. It has no charge with the width of the atomic dimension. The outer layer is called a *diffuse layer,* or *Gouy–Chapman layer* is semi-infinite in nature. It contains unequally distributed cations and anions by following the laws of Poisson and Boltzmann [Oldham, 2008]. The purpose of this work is to develop a basic model to describe the surface potential on the AlGaN/GaN HEMT ion sensors.
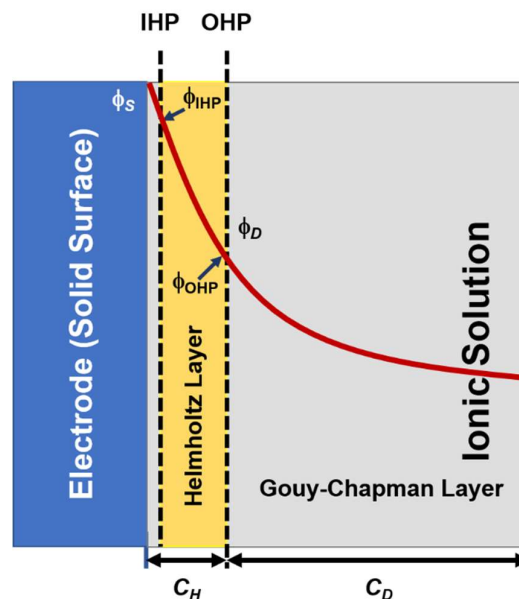

Figure 2.8: Potential and layer representation for Solid/Electrolyte interface modeling

(a) Helmholtz Model

The Helmholtz proposed the concept of an EDL for the first time, and his proposed model is the simplest among all three models [Esposito, 2018]. The Helmholtz concept of EDL dominates in most electrochemical processes that occur at the solid surfaces. The Helmholtz model approximates that ions (anions or cations) attract towards the electrode surface to neutralize the surface charges, i.e., conservation of charge. Consequently, there are two layers of opposite polarity charges, separated by a distance *d*. Therefore, this complete system behaves like a parallel-plate capacitor. Here, the distance *d* is very small and can be approximated as the radius of solvated ions [Bard *et al.*, 1980; Butt and Kappl, 2018]. It separates the charges at the liquid/solid interface. The Helmholtz layer consists of two planes: the inner Helmholtz plane (IHP) and the outer Helmholtz plane (OHP). Here, the space between the surface and the IHP and the space between the IHP and the OHP can be modeled as capacitors, with the capacitances C_1 and C_2, respectively. In many electrical measurements, it is impossible to distinguish the contributions of these capacitances; hence these capacitors are considered as a single Helmholtz capacitance, C_H [Steinhoff, 2008]. In this model, it is important to consider that the surface charges are fixed while the ions in the electrolyte solution are mobile. Thus, the ions present in the electrolyte solution reacts to the surface to change its surface charges. In the Helmholtz model, the Helmholtz or differential capacitance has no voltage dependence. Therefore, it is considered as constant and can be given as [Bard *et al.*, 1980; Steinhoff, 2008]:

$$C_H = \frac{\partial \sigma_S}{\partial \phi_S} = \frac{\varepsilon \varepsilon_0}{d} \tag{2.31}$$

where the σ_S is the surface charge. The capacitance variation indicates that either the dielectric constant of the medium or the distance between two charging layers, d, is not constant. Here, the thickness *d* is approximately a few Angstroms for the Helmholtz electric double layer or Helmholtz capacitance [Esposito, 2018].

The reason for the Helmholtz potential under open circuit conditions is illustrated by Steinhoff for all three types of solid surfaces, including metal, semiconductor, and insulator [Steinhoff, 2008]. In the case of metal surfaces, it is defined by electron transfer between the metal and redox ions in solution. Initially, the difference in the Fermi levels of the metal and electrolyte leads to electron transfer and forms an EDL. At equilibrium, the Fermi levels get equalized, and potential is established. In this case, the adsorption of ions at the surface minorly contributes for the establishment of Helmholtz's potential. At the semiconductor/electrolyte interface, the Helmholtz potential can be either observed by charge transfer reactions to appropriate redox levels in the electrolyte or by adsorption-desorption processes. For non-degenerate semiconductors, this potential is mainly established by adsorption/desorption approaches. The charges in the space charge region of the semiconductor (owing to electron exchange with redox ions) are much smaller than the ionic charges involved in adsorption. In the case of an insulator/electrolyte interface, the surface charges can be observed only from the adsorption of ions or dipoles from the liquid. Hence, in this case, the Helmholtz potential can only be established by adsorption and desorption mechanisms [Steinhoff, 2008].

(b) Gouy-Chapman Model

Gouy and Chapman individually proposed the phenomenon of the diffuse layer. Therefore, this model name is given as the Gouy-Chapman (GC) model [Oldham, 2008]. The detailed derivations are described systematically in literature [Bard *et al.*, 1980]. In the solutions of low ionic concentration, the surface charges of the solid cannot be entirely compensated by the accumulated ions at the OHP. Consequently, a diffuse layer of charges spreading from the OHP into the solution is proposed in the Gouy-Chapman model. In this model, ions are considered as point charges where their polarizability, or the ability of dipole formation immediately, is neglected [Esposito, 2018]. There is a complete electrostatic interaction between ions and the surface and ions, and no chemical reactions or adsorption/desorption occurs at the electrolyte-

semiconductor interface. The electrostatic interaction of the ions and the charged surface is compensated by the random thermal motion. Therefore, the local ion density in the electrolyte at a distance x from the surface can be given by the Maxwell-Boltzmann equation as [Esposito, 2018; Steinhoff, 2008]:

$$n_i(x) = n_i^0 . e^{\left(\frac{-z_i q \phi(x)}{kT}\right)} \tag{2.32}$$

where $n_i(x)$ and n_i^0 are the densities of ions at a distance x, and in bulk respectively, z_i is the charge of the ion i, k is Boltzmann's constant, T is the absolute temperature, and $\phi(x)$ is the potential at a distance x with respect to the bulk solution potential. The relation between $\phi(x)$ and the charge density $\rho(x)$ is given by the 1-D Poisson equation [Bard *et al.*, 1980; Butt and Kappl, 2018; Esposito, 2018; Steinhoff, 2008]:

$$\rho(x) = -\varepsilon\varepsilon_0 \frac{\partial^2 \phi(x)}{\partial x^2} \tag{2.33}$$

By combining Eq. (2.32) and Eq (2.33), the Poisson-Boltzmann equation is observed, which describes potential and charge distribution in the diffuse layer, and it is given as [Esposito, 2018]:

$$\frac{\partial^2(x)}{\partial x^2} = \frac{-q}{\varepsilon\varepsilon_0} \sum_i n_i^0 z_i e^{\left(\frac{-Z_i q \phi(x)}{kT}\right)} \tag{2.34}$$

In the Gouy-Chapman model, the ε is considered as a dielectric constant of electrolyte. Further, in the diffuse layer, the charge per unit area (σ_D) is presented by the modified Graham equation [Rabbaa and Stiens, 2012]:

$$\sigma_D = -(8kT\varepsilon\varepsilon_0 n^0)^{\frac{1}{2}} \sinh\left(\frac{zq\phi_D}{2kT}\right) \tag{2.35}$$

The differential capacitance (C_D) of the Gouy-Chapman layer can be derived by differentiating the above equation and can be given as [Rabbaa and Stiens, 2012; Steinhoff, 2008]:

$$C_D = \left(\frac{2z^2 q^2 \varepsilon\varepsilon_0 n^0}{kT}\right)^{\frac{1}{2}} \cosh\left(\frac{zq\phi_D}{2kT}\right) \tag{2.36}$$

It can be observed from Eq. (2.36) that higher ionic concertation (n^0) or higher differential potential (ϕ_D) causes a strong accumulation of ions and can increase the capacitance C_D. In the Gouy-Chapman theory, the values of differential capacitance are very high and cannot provide a complete explanation for the experimental results. In this regard, the Gouy-Chapman-Stern theory is utilized.

(c) Gouy-Chapman-Stern Model
The Gouy-Chapman-Stern (GCS) model combines the Helmholtz and Gouy-Chapman models [Oldham, 2008]. In this model, the distance between the solid surface and the OHP acts as the Helmholtz model, and the remaining distance from the OHP to the bulk of the electrolyte considered as the Gouy-Chapman model [Bard *et al.*, 1980; Butt and Kappl, 2018; Esposito, 2018; Steinhoff, 2008]. As per the Stern modifications, the Stern or Helmholtz layer signifies the compact layer of immobile ions, is strongly absorbed to the solid surface. There are no free charges or ions available within the Helmholtz layer [Esposito, 2018]. The Gouy-Chapman-Stern model concept is to add both the Helmholtz capacitance and the Gouy-Chapman capacitance together [Esposito, 2018]. The total capacitance is described by the smaller capacitance value of either the Helmholtz, C_H, or the Gouy-Chapman layer, C_D. The total capacitance C_{GCS} in this model can be given as [Steinhoff, 2008]:

$$\frac{1}{C_{GCS}} = \frac{1}{C_H} + \frac{1}{C_D} \tag{2.37}$$

At higher ionic concentration, the C_D of the Gouy-Chapman model can be linearized. Thus, the C_{GCS} can be given as [Steinhoff, 2008]:

$$\frac{1}{C_{GCS}} = \frac{1}{C_H} + \left(\frac{kT}{2z^2q^2\varepsilon\varepsilon_0 n^0}\right)^{\frac{1}{2}} \tag{2.38}$$

In highly concentrated electrolyte, the Gouy-Chapman layer becomes negligibly thick, and most of the charges are situated at OHP. In this condition, the C_{GCS} is dominated by the Helmholtz capacitance C_H. For the solution having a low concentration of the ions, the magnitude of C_D is equal or smaller than C_H. Hence, in this case, the C_D cannot be neglected. From the Eq. (2.35), the surface potential of solid ϕ_S with respect to the bulk solution is given as [Steinhoff, 2008]:

$$\phi_S = -\frac{\sigma_D}{C_H} \mp \frac{2kT}{zq} \sinh^{-1}\left(\frac{|\sigma_D|}{(8kT\varepsilon\varepsilon_0 n^0)^{\frac{1}{2}}}\right) \tag{2.39}$$

2.4.1 Simulation Methodology for Surface Analysis

In the simulation, the simulators generally solve the Poisson's and continuity equations for the analysis of device functionality, as described in the section 2.2. In this case, Poisson's equation for the electrolyte is described as:

$$\nabla.(\varepsilon.\nabla\phi) = -q([M^+] - [A^-]) \tag{2.40}$$

where q is the elementary electron charge, ε is the permittivity of the solution with the product of permittivity of vacuum, and $[M^+]$ and $[A^-]$ are the ionic concentrations of cations and anions, respectively. In the EDL theory, there is an atomic spacing between the inner and outer Helmholtz planes, and the ions cannot physically fit in between these two planes [Esposito, 2018]. It is assumed that the charges between the inner Helmholtz region and outer Helmholtz region cannot be retained; thus, the surface potential in the above equation for this region is given as:

$$\nabla.(\varepsilon.\nabla\phi) = 0 \tag{2.41}$$

Eq. (2.42) and Eq. (2.43) illustrate the continuity equations for cations and anions which describes variations in the ion concentration with respect to time due to drift and diffusion. Here, the first term indicates drift, and the second term explains the diffusion of ions.

$$\frac{\partial[M^+]}{\partial t} = \nabla(q\mu_{M^+}[M^+]\nabla\phi + (D_{M^+}\nabla[M^+])) \tag{2.42}$$

$$\frac{\partial[A^-]}{\partial t} = \nabla(q\mu_{A^-}[A^-]\nabla\phi + (D_{A^-}\nabla[A^-])) \tag{2.43}$$

Further, the Dirichlet boundary conditions are utilized to define the potential at two points: the gate contact of AlGaN/GaN HEMT and the bulk of the electrolyte. The gate contact has surface potential, whereas the electrolyte potential at the bulk is zero as per Grahame's work[Esposito, 2018].

$$\phi|_{x=0} = \phi_S \tag{2.44}$$

$$\phi|_{x=L} = 0 \tag{2.45}$$

In addition, the Poisson's and continuity equations for the AlGaN/GaN HEMT device will be solved similarly as previously described in section 2.2. Moreover, the device structure and physics will also similarly be utilized for device modeling. Hence, this theoretical mathematical modeling for surface analysis, including Helmholtz, GC, and GCS models with Grahame's modifications, implements a realistic theoretical model for AlGaN/GaN HEMT heavy metal ion sensors.

2.5   CHAPTER SUMMARY

In this chapter, a comprehensive analysis was performed with simulation and experimental data that shows validation of the simulation process by utilizing the Sentaurus TCAD simulator tool. Device parameters such as mobility, piezoelectric polarization, surface trap concentration, and contact resistance, and many more were observed by simulation along with the electrical characteristics of the device. Moreover, the self-heating of the device is also analyzed by employing thermal boundary conditions. The impact of self-heating can also be realized in the degradation of the I_{DS} at the higher electric field. In addition, fundamental modeling for the surface analysis was also performed for the heavy metal ion sensing applications. This modeling gives a theoretical overview of the solid/electrolyte interfacing using Helmholtz, Gouy-Chapman and Gouy-Chapman-Stern models, which help in the surface analysis of AlGaN/GaN HEMT based heavy metal ion sensor.

…